Analysis of an optical millimeter wave generation RoF system using pre-distortion and FBG techniques

SUGANTHI SANTHANAM*, T. KRISHNA MARI SELVI*
Department of Electronics and Communication Engineering, K. Ramakrishnan College of Technology, Tiruchirappalli, Tamilnadu, India

This work investigates the effect on the optical millimeter (mm)-wave long-haul RoF with pre-distortion systems and Fiber Bragg grating (FBG) techniques. Dual-Drive Mach-Zehnder Modulator (DDMZM) is used to generate the long-distance but inexpensive RoF mm-wave-based system by varying transmission rates of 1, 5, and 10 Gbps and power parameters of 0, 5, 10, and 15 dBm, respectively. Graphical analysis is done for Q-factor, Bit Error Rate (BER), and eye height with a 140 Km fiber link at a 10 Gbps bit rate. The results demonstrate that the system achieves excellent performance with a high Q-factor, low BER, and well-opened eye diagrams, confirming its feasibility for high-capacity and long-distance wireless access networks. Furthermore, the combination of pre-distortion and FBG techniques provides a scalable, low-cost, and energy-efficient solution, making the design highly suitable for next generation.

(Received March 12, 2025; accepted February 2, 2026)

Keywords: Millimeter-Wave, Radio over Fiber, Pre-distortion, Fiber Bragg Grating, Non-Return-to-Zero, Dual-Drive Mach-Zehnder Modulator, Single-Mode-Fiber

1. Introduction

Optical fiber has grown into a reliable and efficient way to interact in the era of modern communication. The basic principle of the global development and implementation of light-wave systems is the enormous possible bandwidth of optical communications networks. Dispersion causes the light pulses to enlarge as they pass through a fiber optic, often referred to as the broadening of pulses while they pass via the fiber, which reduces the efficiency of the system. For instance, modal multimode fiber usually experiences distortion, as shown in Fig. 1, because of its wide core diameter, which allows it to carry multiple modes that follow distinct courses. As a result, a short pulse with many modes will disperse, since each mode will arrive at its destination at a different time.

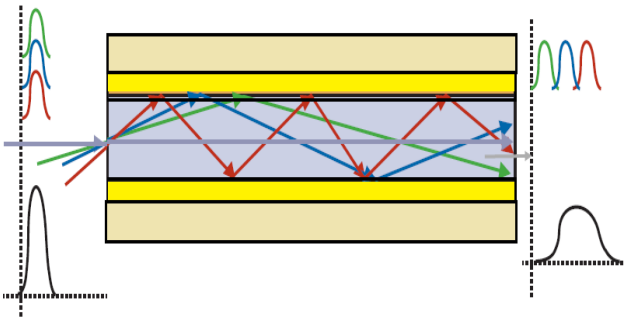

Fig. 1. Iillustration of modal dispersion distortion (colour online)

The optimization of power and fiber dispersion has been studied with correction's effects on optical transmission systems using NRZ and RZ modulation [1] with Dispersion Compensating Fiber (DCF) in 5, 10, 15, 20, and 25 Km along with power parameters 0, 5, 10, and 15 dBm. In continuation with this, prior to the frequency up-conversion, fiber and fiber Bragg grating were employed [2] as dispersion compensation, and as a result, optical receivers, the BER, Q-factors of system performance of PIN, and ultrafast APD were examined. The bit error rate of 5 Gbps with 140 Km fiber [3] connected across 60 GHz mm-wave and the 15 GHz local oscillator. $2.05e^{-18}$ of BER and 8.67 Q-factor are obtained and reported. An efficient pre-distortion method was employed in reducing the problems for analogue RoF [4] systems caused by merging that occurs between the optical channel's chromatic dispersion and the laser source's frequency chirp. The authors in [5] demonstrated the generation of a full duplex mm-wave using the RoF system simulation setup using FBG that contrasts the noise and output power signal levels of several light modulators to generate mm-waves that are stable and noise-free optical technology must be used in 5G communication networks. A 160 GHz mm-wave signal was generated by a 10 GHz local oscillator, and 16 tuples at 5 Gbps of data across a 100-Km distance [6] for single sideband suppressed carrier have been proved with a 0.922 dB power penalty, a signal value Q-factor of 5.14, and a BER of 10^{-9}. An optical communication system has been presented to operate in C-band using [7] cascaded FBGs of different lengths, and dispersion compensation has been achieved by use of the apodization-chirped FBG that does non-return to zero [8]. The investigation was done for the study of the impact of chirped FBG with dual apodization functions and dispersion compensating items of linear and quadratic chirps [9]. A typical 10 Gbps fiber optic

connection over 100 Km long distance was used in [10] to assess the strategies and at the users end of frameworks. The offered model improves its presentation for the [11] Q-factor above 18. By changing three distinct parameters, the attenuation coefficient (dB/km), power input (dBm), and length of channel (Km) have been evaluated for [12] system's performance, which was reported using measurements of the BER analyzer, BER, power output (dBm), optical SNR output (dB), gain (dB), noise figure (dB), and signal Q-factors. The authors in [13] improved the dispersion compensating performance in Chirped FBGs (CFBGs) by optimizing the apodization profile.

An 8x1 Wavelength Division Multiplexing (WDM) Multi Input Multi Output (MIMO) communication system with optical grating techniques [14] using a data rate of 5 Gbps was reported with higher BER and Q-factor values [15] obtained by marginally costly Dispersion Compensating Fiber (DCF). To enhance FBG performance with the highest gain, power output with Q-factors [16] has been used in Dense Wave Length Division Multiplexing (DWDM). A linear-chirped CFBG, with [17] a 90-mm short grating length, optimized the model's performance, and the investigation reported dispersion difficulties in wavelength division multiplexing transmission [18] system by utilizing three types of FBGs at different optical bands. Based on a 90 Km fiber, it seems that the system operates rather effectively at 5 Gbps transmission of data with a Q-factor of 30.8 [19]. With long-distance optical communications networks [20], the effectiveness of WDM and Time Division Multiplexing (TDM) was investigated. The issues that RoF technologies will have in the future to sustain networks beyond 5G [21] and their requirements are compiled in this investigation, which also examines the technologies recent and historical advances. Some standardization organizations, including [22] the International Telecommunication Union (ITU), the Asia-Pacific Tele community (APT), and the International Electrotechnical Commission (IEC), have carried out standardization initiatives involving RoF technologies and systems. In contrast to Stimulated Raman Scattering (SRS) [23] which induces transfer of noise in single mode fibers, which severely degrades them, 5G New Radio (NR) signals with various modulation formats are successfully transferred across hollow-core fibers and multicore fibers without degradation when a power-over-fiber and 5G NR analog RoF link are combined in a single fiber. Power over fibers ability to transform power delivery and management in crucial applications [24] by providing a reliable solution with low noise, optimal efficiency, and excellent isolation is highlighted in this study, which also demonstrates the research and development effort of power over fibers under difficult environments. The WDM-RoF system with bit rate changes was analyzed [25] in this investigation to identify the bit rate value that still complied with the standard. External modulation visualizes such as BER analyzers, optical spectrums, and eye diagrams are used to confirm [26] the quality of the signal sent over the optical fiber. Advanced modulation formats like OFDM and QAM [27] increase performance by lowering susceptibility to noise and dispersion and increasing spectral efficiency and data rates. In a fiber-wireless access system that converges both fiber and wireless technologies, with 3×1.333 Gbps dynamic transmissions across a 10 Km fiber channel and a 5 m, 38 GHz mm-wave wireless link, [28] numerous experiments are conducted to investigate the network performance and optimal network architecture. The integrated solution that this study suggests, integrating mm-wave and optical technologies, aims to solve these issues [29] by streamlining the base station and centralizing processing duties. A comb with variable line spacing and multiple spectrum-flat lines with low phase noise (−88.5 dBc/Hz at 1 kHz offset and −108.3 dBc/Hz at 100 kHz offset) are produced [30] by the DD-MZM implementation. Using N = 2 as an example, [31] ultimately generated an 80-GHz 4-QAM W-band mm-wave using 2-ASK signals and finished its high-performance transmission across a 1-m wireless link. 6.93 Gbps is sent over 10 m of fiber plus 2 m wirelessly in the experimental proof provided, [32] using a data stream that complies with the IEEE 802.11ad WLAN standard in a single 60-GHz frequency band. A dual-band Bandpass Filter (BPF) with a wide frequency ratio is suggested [33]. A 3.5/28-GHz Bandpass filter is used for demonstration.

Dispersion compensation can be achieved using different techniques such as DCF, FBG, and Pre-distortion.

- In the DCF method, a section of negative-dispersion fiber is inserted after the transmission span of Single-Mode Fiber (SMF), where the positive dispersion accumulated in the SMF is effectively canceled by the negative dispersion of the DCF, thus restoring pulse integrity before detection.
- Alternatively, FBGs can be used as a compact dispersion compensator, where a chirped FBG introduces wavelength-dependent delays that counteract the pulse broadening caused by SMF dispersion; this approach offers low insertion loss and requires less physical space compared to long DCF modules.
- A third approach is the pre-distortion method, where the transmitted signal is intentionally distorted in amplitude and phase at the transmitter side such that, after experiencing fiber-induced dispersion and nonlinearity, the received signal is reconstructed in its original undistorted form.

Together, these methods represent effective compensation strategies, with DCF providing fiber-based compensation, FBG offering grating-based compact compensation, and pre-distortion enabling transmitter-side correction.

In this paper, to mitigate dispersion effects, two methods, pre-distortion and FBG have been proposed. The 30 and 60 GHz mm-wave generation is carried out with RoF having DDMZM, and a 30 and 60 GHz RF local oscillator with an optical fiber length ranging from 10 to 140 Km and a rate of data transfer of 1, 5, and 10 Gbps has been used for six different modules (basic mm-wave, pre-distortion, pre-FBG, post-FBG, pre-distortion pre-FBG,

and pre-distortion post-FBG). The characterization and comparison are made among all proposed modules and proved that the pre-FBG mm-wave of the RoF system has achieved low BER and high-power output, bandwidth, and Q-factor for contemporary wireless network applications.

2. Theoretical background of RoF

The optical fiber's chromatic dispersion, phase noise, and nonlinearity are the impairments that typically restrict the radio over fiber performance of the system owing to the transfer of analog data in the fiber. Here, the summary of the main categories of RoF system impairments has been presented.

2.1. RoF impairments & compensation

Chromatic dispersion broadens the pulses by causing different wavelengths to go at different speeds and is reduced by employing methods such as DCF and FBG. Pre-distortion methods are essential for enhancing fiber communication system performance, and it involves altering the properties of a light pulse prior to its introduction in an optical fiber link. It could entail employing sophisticated coding techniques or chirping the frequency to counteract non-linearity for RoF networks and increase power efficiency; pre-distortion improves the linearity for transmitter amplifiers. Another popular method for dispersion compensation is FBG, which is produced by consistently altering the core refractive index, resulting in a brief segment of optical fiber, typically a few centimeters in length. Numerous approaches, including core scanning, and interferometric, as well as direct point-by-point methods, can be used to build it. In optical fiber networks, FBG aids in overcoming nonlinear impairments and inherent dispersion. Utilizing FBG to act as a dispersion compensating module increases the efficiency of long-distance transmission.

Formats for higher-order modulation are more susceptible to nonlinear effects and signal distortion. FBG dispersion correction is more effective for simpler formats such as BPSK, (Binary Phase Shift Keying) QPSK, or (Quadrature Phase Shift Keying), and it can assist in correcting the dispersion of colors in those high-order systems of Quadrature Amplitude Modulation (QAM) such as 16-QAM, and 64-QAM. However, the accuracy of the compensation determines how effective it is. Although chromatic dispersion rises with fiber length, its effects are usually less pronounced at lower frequencies, which means that pre-distortion is usually not as necessary. In contrast, the FBGs must be quite precisely built in order to control dispersion for these higher frequencies.

2.2. Basic mm-wave in RoF system

Optical external modulation proved to be a successful method for optical transport at greater frequencies, including mm-wave transmissions. Utilizing an external modulator, such as the MZM and the laser operates in continuous wave mode. By biasing the MZM to a suitable value, the half-wave voltage that suppresses a light carrier in the centre of the wavelength can be controlled, and the pulses of both the upper and lower first side modes at a frequency twice larger than the mm-wave signal were employed by the MZM at the required mm-wave signal. The basic RoF system circuit layout is displayed in Fig. 2.

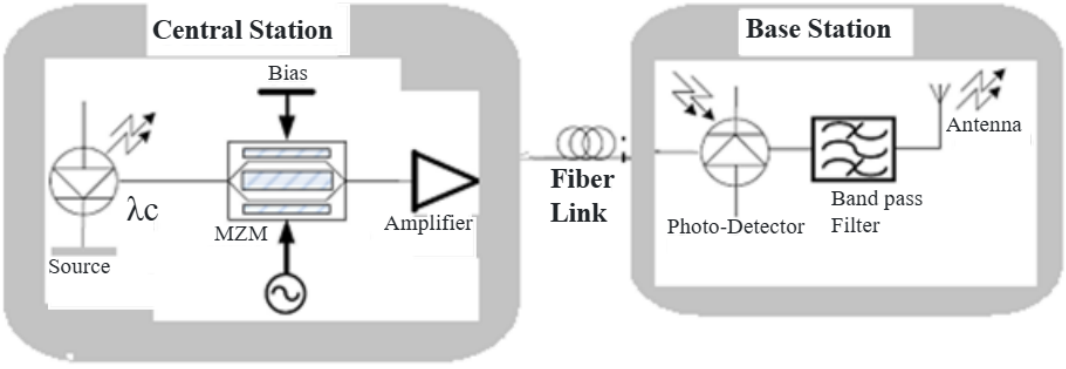

Fig. 2. Basic RoF system

2.3. Pre-distortion mm wave RoF system

Fig. 3 depicts a traditional linearly modulated RoF link with the suggested pre-distorter included, in which the optical fiber line, a photodiode that transforms optical power into electrical current, and a laser transmitter make up the RoF link. The combined effects of fiber chromatic dispersion and laser chirp lead to signal loss in RoF networks. Pre-distortion techniques in mm-wave RoF systems are used to compensate for nonlinearities in optical and electrical components, improving signal quality and system performance.

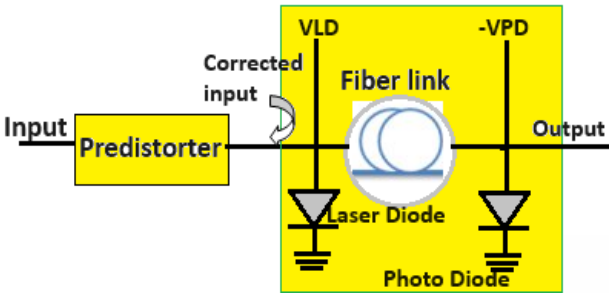

Fig. 3. RoF link with a pre-distorter (colour online)

In the RoF system, nonlinearities arise due to MZM nonlinearity causing signal distortion due to its transfer function. Optical pre-distortion is to be implemented at the optical transmitter to compensate for MZM nonlinearity. It involves signal pre-processing before optical modulation. Electrical pre-distortion (EPD) is applied before the modulator or power amplifier. It compensates for RF and electrical nonlinearities. This can be implemented digitally or using analog circuits.

2.4. Pre-FBG and post-FBG mm-wave RoF system with and without pre-distortion

FBG-based dispersion compensators have the potential for more compactness than DCF compensators, and they may also have less optical nonlinearity and insertion loss [8]. This function can increase the optical signal-to-noise ratios while lowering system costs. A dispersion tuning range that includes, for most applications, both the positive and negative values is required and is the main advantage of FBG technology over DCF. By altering the fiber grating's physical properties, a specific bandwidth, width, or other feature can be achieved, as shown in Fig. 4 with pre- and post-FBG in (a) and (b) correspondingly, and pre-distorter and pre-FBG and pre-distorter post-FBG in (c) and (d).

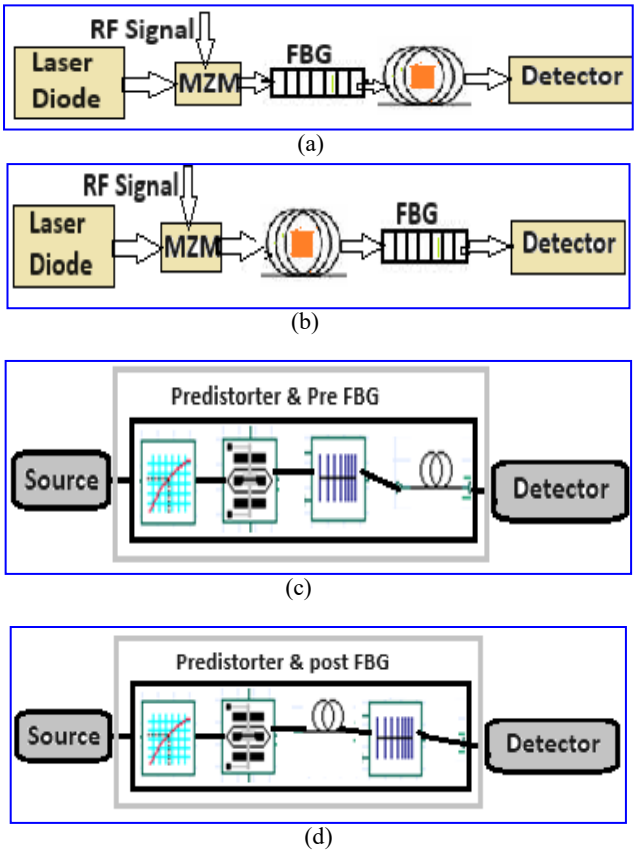

Fig. 4. Mm-wave RoF system with & without PR distorter including (a) pre-FBG, (b) post-FBG, (c) pre-FBG, with pre-distorter including, (d) post-FBG, with pre-distorter including, (colour online)

3. Mathematical analysis of simulation components

3.1. Modulator

In Fig. 5, a DD-MZM basic model is presented, which can be used with light transmission of $LiNbO_3$ crystals of length L at d distance between plates of each electrode. If an electric field's strength, E, is situated between the electrodes [7], the refractive index of its plates is as given in eq. (1).

$$n = n_0 \frac{1}{2} n_0^3 PE \tag{1}$$

E and P represent the electro-optics effect coefficient, while n_0 represents the refractive index of light. Moving back to E's conversional eq. (2):

$$E = v \mid d \tag{2}$$

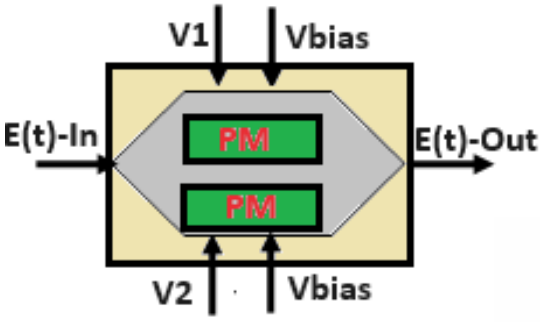

Fig. 5. DD-MZM (colour online)

That leads to

$$n = n_0 - \frac{1}{2} n_0^3 P(d) \tag{3}$$

An incident optical wave's optical field is

$$\psi_{(t,0)} = \psi_{in}(t) = A_0 \exp(-j2\pi f_c t) \tag{4}$$

Next, for L distance

$$\psi_{in(t,L)} = A_0 \exp(-j2\pi f_c t - \phi) \tag{5}$$

where

$$\phi = \frac{2\pi nL}{\lambda_0} = \frac{2\pi nL}{\lambda_0}\left(n_0 - \frac{n_0^2 pv}{2d}\right) = \phi_0 - \Delta\phi \tag{6}$$

where, the distance at which the used electric voltage (v) changes constantly is represented by ϕ_0. Next,

$$\Delta\phi = \frac{\pi L n_o^3 pv}{\lambda_0 d} \tag{7}$$

As a result, the phase change is $\Delta\phi$. A switching voltage (V_π), also referred to as the half-wave voltage, is the voltage required [7] to achieve a phase transition π.

$$\Delta\phi = \pi = \frac{\pi L n_o^3 p v V_\pi}{\lambda_0 d} \quad (8)$$

$$V_\pi = \frac{\lambda_0 d}{L n_o^3 p v};$$

$$\psi_{in}(t, L) = A_0 \exp\left[-j\left(2\pi f_c t - \phi_0 + \frac{\pi V}{V_\pi}\right)\right] \quad (9)$$

Thus, there is a direct correlation between the phase change and the applied voltage. In the case where V (t) represents the message signal, the optical carrier's phase can be adjusted to match it. The electromagnetic field that enters the shorter or upper arm of the interferometer [7] if a source of losses is ignored is

$$E_{upper,lower} = \frac{A_0}{\sqrt{2}} \exp(-j2\pi f_c t) \quad (10)$$

To keep the total power constant, the factor $1/\sqrt{2}$ is used. When the voltages applied (V_1 and V_2) are present, optical beams in the upper and lower arms experience a phase shift of ϕ_1 and ϕ_2. Therefore, by using eqs. (6) to (10) together, we obtain:

$$\phi_j = \frac{2\pi L}{\lambda_0}\left(n_0 - \frac{1}{2} n_0^3 p v_j(t)/d\right) \quad (11)$$

where, j= (1, 2) = $\phi_0 \frac{-V_j \pi}{V_\pi}$

These optical beams lower and top arms are

$$\psi_j = \frac{A_0}{\sqrt{2}} \exp\left[-j\left(2\pi f_c t - \phi_j\right)\right] \quad (12)$$

The output of the second branch is $\psi_{out} = \frac{\psi_1 + \psi_2}{\sqrt{2}}$

Therefore,

$$\psi_{out} \frac{A_0}{\sqrt{2}} \exp\left(-j_\pi f_c\left[\frac{\exp(j\phi_1)}{\sqrt{2}} + \frac{\exp(j\phi_2)}{\sqrt{2}}\right]\right) \text{ and}$$

$$A_0 = A_0 \exp\left[\frac{j(\phi_1 + \phi_2)}{2} * \frac{\exp\left[j(\phi_1 - \phi_2)/2 + \exp\left[j(\phi_1 + \phi_2)/2\right]\right.}{2}\right] \quad (13)$$

$$A_{out} = A_0 \exp(j\bar{\phi}) \cos\left[\frac{v_1(t) - v_2(t)\pi}{2v_\pi}\right] \quad (14)$$

3.2. Pre-distorter

For an instantaneous frequency shift or chirp

$$W_r = \frac{-d\bar{\phi}}{dt} = \frac{\pi}{2v_\pi}\left(\frac{dV_1}{dt} + \frac{dV_2}{dt}\right) \quad (15)$$

The optical power output is

$$P_{out} = |A_{out}|^2 = P_0 \cos^2\left[\frac{[V_1(t) + V_2(t)]\pi}{2V_\pi}\right] \quad (16)$$

And to have zero chirp $\frac{dV_1(t)}{dt} = \frac{-dV_2(t)}{dt}$ and $V_1(t) = -V_2(t) + V_{bias}$

where, V_{bias} is a voltage that constantly changes. By assigning the messages signal m (t) to V_1 (t), the output power having constant phase shift [7] is

$$P_{out} = P_0\left[\left[m(t) - \frac{V_{bias}}{2}\right]\frac{\pi}{V_\pi}\right] \quad (17)$$

$$Or\ A_{out} = A_0 \cos\left[\left[m(t) - \frac{V_{bias}}{2}\right]\frac{\pi}{V_\pi}\right] \quad (18)$$

Consequently, when $V_{bias}=V_\pi$ is taken into account, eq. (18) is

$$A_{out} = A_0 \sin\left[\frac{m(t)\pi}{V_\pi}\right] \quad (19)$$

where $(t)/v_\pi \ll 1$

$$\psi_j = \left(\frac{A_0 \pi}{V_\pi}\right) m(t) \exp\left[-j2\pi f_c(t)\right] \quad (20)$$

MZM now functions as a product modulation; as a result,

When $[v_{bias} = v_\pi/2]$

$$A_{out} = A_0 \cos\left[\frac{m(t)\pi}{V_\pi} - \frac{\pi}{4}\right]$$

$$A_{out} = \frac{A_0}{\sqrt{2}}\left[\cos\left[\frac{m(t)\pi}{V_\pi}\right] + \sin\left[\frac{m(t)\pi}{V_\pi}\right]\right] \quad (21)$$

When $(t) << V_\pi/\pi$

$$\cos\left[\frac{m(t)\pi}{V_\pi}\right] = 1 \text{ and } \sin\left[\frac{m(t)\pi}{V_\pi}\right] = \frac{m(t)\pi}{V_\pi}$$

Therefore,

$$\psi_{out} = \frac{A_0}{\sqrt{2}}\left[1 + \frac{m(t)\pi}{V_\pi}\right]\exp(-j2\pi f_c) \quad (22)$$

In the above equation, let m (t)=[+v for bit "1"-v for bit "0"]

The pre-distortion's output [7] is

$$V_{out}(t) = \frac{1}{\pi}\sin^{-1}(V_{in}(t)) * a + b \quad (23)$$

Assume a=1 and b=0. Therefore, Pre-distortion's output is

$$V_{out} = \frac{1}{\pi}\sin^{-1}(V_{in}(t)) \quad (24)$$

Table 1. The properties and the impact of various techniques

Property	Definition	Impact	Applications
Grating Period	The distance in the fiber between successive modulations of the refractive index	The precise wavelength known as the Bragg wavelength is determined by the grating period.	WDM
Refractive Index Modulation	Modification of the fiber core's refractive index	Impact the FBG's bandwidth and reflectivity. Stronger the reflection, the higher the modulation.	Optical filtering and signal stabilization.
Grating Length	The fiber section length was measured at the engraved grating.	Affects the reflected signal's bandwidth. Shorter gratings result in wider reflection spectra, and longer gratings have narrower reflection bandwidths.	Wavelength filtering. Shorter gratings & sensing
Apodization	Gradual shift in the modulation in the refractive index along the FBG's length.	It reduces the side lobes in the FBG's reflection spectrum, leading to a cleaner signal with less interference.	Dense WDM systems
Chirping	Changing the grating duration over the FBG's whole length.	Chirped FBGs produce a wider reflection spectrum since they reflect a variety of wavelengths as opposed to only one.	dispersion compensation
Thermal Sensitivity	FBG's response to temperature changes	Shifts in the Bragg wavelength, potentially causing signal degradation if not managed properly.	Sensing
Strain Sensitivity	FBG's response to mechanical strain	Alters the grating period and refractive index.	Wavelength tuning and fiber integrity mentoring
Pressure and Environmental Sensitivity	FBGs react to changes in external pressure and environmental conditions	Shift the Bragg wavelength, affecting the system's performance.	Sensing

$$m(t)=\frac{1}{\pi}\sin^{-1}\left(-V_{in}(t)\right), bit=0; \frac{1}{\pi}\sin^{-1}\left(V_{in}(t)\right), bit=1$$

Let MZM's P_{out} be

$$P_{out1}=P_0\cos^2\left[\frac{m(t)\pi}{V_\pi}-\frac{V_{bias}\pi}{2V_\pi}\right] \quad (25)$$

At logic 0

$$P_{out1}=P_0\cos^2\left[\frac{\frac{1}{\pi}\sin^{-1}\left(V_{in}(t)\right)\pi}{V_\pi}-\frac{V_{bias}\pi}{2V_\pi}\right] \quad (26)$$

At logic 1

$$P_{out1}=P_0\cos^2\left[\frac{\frac{1}{\pi}\sin^{-1}\left(-V_{in}(t)\right)\pi}{V_\pi}-\frac{V_{bias}\pi}{2V_\pi}\right] \quad (27)$$

3.3. Chirped fiber Bragg grating

FBGs are vital parts of optical networks and communication systems due to their ability to selectively reflect specific wavelengths of light while transmitting others. Their physical properties determine their functionality and applications in these systems. The important properties and their impact are listed in Table 1.

Bragg Wavelength (λ_B): The FBG's most effective wavelength for light reflection is known as the central, or Bragg, wavelength, or λ_B. The grating period (Λ) and the fiber core's effective refractive index (n_{eff}) define it and given as

$$\lambda_B = 2n_{eff}\Lambda \quad (28)$$

In this case, Λ is the grating period or the separation between successive grating planes, and n_{eff} is the fiber core's effective refractive index.

Grating Reflectivity: The amount of light reflected by a grate at the wavelength of Bragg is measured by an FBG's reflectivity, or R. It is dependent on the index modulation Δn, the coupling constant κ, and the grating length L.

$$\mathrm{R} = \tanh^2(\mathrm{kL})$$

where κ is the coupling coefficient, given by

$$k = \frac{\pi.\Delta n}{\lambda_B} \tag{29}$$

The variation between the grating's greatest and lowest refractive indices is known as the index modulation, or Δn, while L is the grating's length.

Bandwidth of the FBG (Δλ): The bandwidth of the FBG, i.e., the range of wavelengths over which significant reflection occurs, is determined by the length of the grating and the coupling coefficient

$$\Delta\lambda = \frac{\lambda_B}{n_{eff}}.\frac{1}{L} \tag{30}$$

Reflectivity Spectrum: The reflectivity spectrum of an FBG describes how reflectivity varies with wavelength around the Bragg wavelength. The spectrum is influenced by grating profile (e.g., uniform, apodised, chirped) and the index modulation. For a uniform grating, the reflectance with respect to wavelength (λ) can be approximated by

$$R(\lambda) = \tanh^2 \frac{\left(kL\sqrt{1} - \left(\frac{\lambda - \lambda_s}{\Delta\lambda}\right)^2\right)}{1 + \left(\frac{\lambda - \lambda_s}{\Delta\lambda}\right)^2} \tag{31}$$

Apodization and Chirping: Adjusting the index of modulation Δn across the grating in order to lessen the sides in the spectrum of reflection is known as apodization. Along their whole length, chipped FBGs have a variable grating period, Y(z). Dispersion adjustment in optical fibers can be achieved by using this, which broadens the reflection spectrum. The rate of variation over the grating period is known as the chirp rate C.

$$C = \frac{d\Lambda}{dz} \tag{32}$$

Along the grating, the Bragg wavelength is given by

$$\lambda_B(z) = 2n_{eff}\Lambda(z) \tag{33}$$

Transmission Spectrum: The transmission spectrum of an FBG is complementary to its reflection spectrum. It shows the wavelengths that pass through the grating with minimal attenuation. For a uniform FBG, the transmission T (λ) has the following expression:

$$T(\lambda) = 1 - R(\lambda) \tag{34}$$

In summary, the physical properties of FBGs, such as the grating period, refractive index modulations, and sensitivity to environmental factors, play a vital role in their functionality within optical communication and networking systems. These properties allow FBGs to perform critical tasks like wavelength filtering, dispersion compensation, and real-time sensing, making them indispensable in modern optical networks. Fig. 6 illustrates a chirped grating structure using length L_g, grating time Λ_0, and chirped bandwidth $\Delta\lambda_{chirp}$. The variance of a chirp provided by the variation across shorter and longer wavelengths is given [14] in eq. (35).

$$\lambda_{chirp} = 2n_{eff}\left(\Lambda_{long} - \Lambda_{short}\right) = 2n_{eff}\Delta\Lambda \tag{35}$$

where the effective refractive index is denoted by n_{eff}.

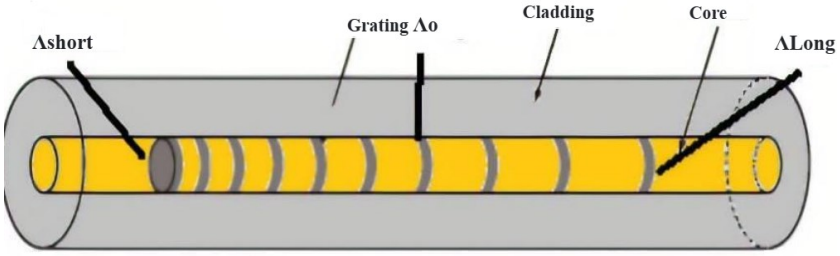

Fig. 6. Chirp fiber grating schematic (colour online)

Eq. (36) gives the chirped FBG's dispersion, Dg, which is connected with the fiber grating's n_{eff} length (l) and chirp variation ($\Delta\lambda_{chirp}$).

$$D_g = \frac{2n_{eff}}{\Delta\lambda_{chirp}c}l \tag{36}$$

where light travels at a speed of c. Refraction causes light encountering a chirped FBG to delay by τ, and dispersion results from the greatest delay of $2L_g/V_g$ between the longest and shortest wavelengths, as determined by [14] and provided by

$$\tau(\lambda) = \frac{(\Lambda_0 - \Lambda)}{\Delta\lambda_{chirp}c}.\frac{2L_g}{V_g} = \frac{D_g(\Lambda_0 - \Lambda)}{2n_{eff}l}.\frac{2L_g}{V_g} \tag{37}$$

When Λ_0, the Bragg wavelength at the center of the chirped bandwidth of a grating, is the Bragg wavelength and Vg is the group's speed of light within the fiber. The development of eq. (4), which link the fiber delay with the total chromatic dispersion, or D_{ch}, across a fiber length L, is done in [7].

$$\frac{\Delta\lambda}{L} = D_{ch}(\Delta\lambda) \tag{38}$$

where the source spectrum's limited width is represented by (ΔΛ). The Bragg wavelength ΓB(z) that crosses the core of a chirped fiber grate is given by [13] eq. (37) when a frame in references for the +z direction is taken into account and given a refractive index, n(z).

$$\Lambda B(z) = 2n(z)\Lambda(z) \tag{39}$$

The following represents a linear fluctuation from period's Λ_0 to Λ (z):

$$\Lambda(z) = \Lambda_0 + xz \tag{40}$$

As expressed in [12] by eq. (41): an apodization function g(z), a mean variance of the index modulation Δn, and an effective index n_{eff} of the fiber all influence a refractive index n (z).

$$n(z) = n_{eff} + \Delta n.g(z)\cos\left(\frac{2\pi z}{\Lambda_0}(1+xz)\right) \tag{41}$$

Eventually, the BER, Q-factor, and optical to signal noise ratios are the key metrics that characterize a transmission link's performance as deduced from the eye diagrams. The following parameters are considered in determining the OSNR: input power P_{in}, total dispersion D_t, amplifier noise figure N_f, the optical fiber attenuation coefficients α and dispersion coefficient D_f, frequencies υ, and the bandwidth frequency $\Delta_{\upsilon 0}$ [11].

$$OSNR = \frac{P_{in}D_f}{N_f h\nu\Delta_{\nu 0}\alpha(D_t + D_g)} \tag{42}$$

h is the symbol for Planck's constant. The OSNR, optical bandwidth B_0, and the electrical bandwidth of the receiving filter B_c are the factors that determine the quality factor, according to [12].

$$Q = -\frac{OSNR}{\sqrt{2}OSNR + 1 + 1}\sqrt{\frac{B_0}{B_c}} \tag{43}$$

The following techniques are used to calculate the BER performance of the chosen apodization profile:

$$BER = 0.5erf\left(\frac{Q}{\sqrt{2}}\right) \tag{44}$$

Bragg's gratings are utilized in chromatic dispersion compensation in fiber transmissions, and a variety of apodization functions are employed to enhance transmission performance [17]. According to [16], chirped gratings provide the best characteristics to ensure linear compensation of dispersion in fibers, while apodization lessens the impacts of internal interference caused by group delay. The chromatic dispersion correction performance of the suggested design is assessed using the Gaussian apodization function for the specified refractive indices (n = 1.46). The function g(z) for Gaussian apodization is as follows:

$$g(z) = \exp\left(-\alpha\left(\frac{z}{l} - 0.5\right)^2\right) \tag{45}$$

where the apodization strength is represented by a and the grating length parameter by x. 25. 0 < z < l; 0≤ x ≤ L1 ≤ a.

4. Simulation setup

Six distinct modules (pre-distortion, pre-FBG, post-FBG, pre-distortion pre-FBG, and pre-distortion post-FBG) are shown in this analysis using a low-cost (one DDMZM) mm-wave in a RoF system. Tables 2 to 7 list the simulation settings, optical fiber characteristics, and FBG fiber parameters in that order. Continuous-Wave (CW) operation refers to a laser's ability to pump and produce light constantly. The wavelength has been used to calculate the CW laser's frequency. A wavelength of 1550 nanometers is represented by λ, and the speed of light, c, is 3×10^8 m/s.

$$f = \frac{c}{\lambda} = \frac{3\times10^8}{1550\times10^{-9}} = 193.5\times10^{12}Hz \tag{46}$$

The wavelength of 1550 nm is roughly 193.5 THz, which is the center frequency. CW lighting in this frequency is used as the light source in a basic millimetre-wave RoF system as shown in Fig. 7 (a), and a polarization controller is placed at the transmitting end in the simulation setups. The Extinction Ratio (ER) which measures the effectiveness of the modulator in distinguishing between the "on" and "off" states of the optical signal, typically expressed in dB is chosen as next controlling parameter and is given by

$$ER(linear) = \frac{P_{on}}{P_{off}} \tag{47}$$

where $P_{on}$is the optical power when the modulator is fully transmitting (constructive interference, typically when V=0, P_{off} is the optical power when the modulator is fully blocking (destructive interference, typically when $V=V_\pi$.

For a MZM, the output optical power can be written as

$$P_{out} = P_{in}\cos^2\left(\frac{\Delta\phi}{2}\right) \tag{48}$$

The phase difference caused by the voltage being applied is denoted by Δϕ, while Pin represents the optical power input. For the "on" state, when $V = 0, \Delta\phi = 0, P_{on} = P_{in}\cos^2\left(\frac{0}{2}\right) = P_{in}$ and for the "off" state, when

$$V = V_\pi, \Delta\phi = \pi, P_{off} = P_{in}\cos^2\left(\frac{\pi}{2}\right) = 0 \tag{49}$$

In reality, due to imperfections and incomplete destructive interference, P_{off} is not exactly zero but rather a small residual power. In dB, the ER is expressed by:

$$ER(dB) = 10\log_{10}\frac{P_{on}}{P_{off}} \tag{50}$$

P_{on} = 1 mW = 0 dBm and P_{off} = 10 μW = -20 dBm. The extinction ratio in dB is

$$ER(dB) = 10\log_{10}\frac{1mW}{10\mu W} = 10\log_{10}(100) = 20dB$$

The Pockels reaction is observed in the refractive index of the LiNb crystal, which changes linearly with applying an electric field. The change in the refractive index, Δn, is calculated using

$$\Delta n = -\frac{1}{2}n^3 r_{33}E \tag{51}$$

LiNb's refractive index is denoted by n, its electro-optic coefficient, r_{33}, is usually ~30.8×10^{-12}m/V, and the electric field that is applied is represented by E.

The phase shift induced in the MZM arm due to the applied voltage is:

$$\Delta\phi = \frac{2\pi}{\lambda}L\Delta n \tag{52}$$

where L is the modulator's arm length and λ is the light's wavelength (measured in meters). When Δn is substituted,

$$\Delta\phi = -\frac{\pi}{\lambda}n^3 r_{33}LV \tag{53}$$

The electrical field E is proportional to the applied voltage V and is expressed as E = V/d, where d is the electrode gap. Determining the voltage necessary to cause a shift in phase of π radians, or Vπ, is essential for assessing the MZM's efficiency.

$$V_\pi = \frac{\lambda}{n^3 r_{33}L} \tag{54}$$

This is a key parameter for designing and simulating MZMs as it determines the voltage swing needed to switch the modulator. The output optical power $P_{out\ of}$ the MZM, given the input power P_{in}, can be described by:

$$P_{out} = P_{in}\cos^2\left(\frac{\Delta\phi}{2}\right) \tag{55}$$

With Δϕ depending on the applied voltage:

$$P_{out} = P_{in}\cos^2\left(\frac{\pi V}{V_\pi}\right) \tag{56}$$

The MZM's transfer function relates the input electrical signal to the output optical power:

$$E_{out} = E_{in}\cos\left(\frac{\Delta\phi}{2}\right) \tag{57}$$

The optical signal's input and output electric fields are denoted by E_{in} and E_{out} in this instance. The electrode configuration and velocity matching of the RF and optical signals are factors that affect the modulator's bandwidth B.

$$B \approx \frac{c}{2nL} \tag{58}$$

where the refractive index is represented by n and the speed of light by c. A NRZ pulse generator, a 10 Gbps random modulation approach, a 90 GHz sine wave generator, and a pseudo-random bit sequence generator were used to apply two RF-applied voltages to the upper and lower arms of the LiNb MZM modulator, which has an ER of 20 dBm. The optical amplifier, which has a gain of 20 dB and a noise level of 4 dB, has been utilized to amplify the MZM output. Each optical pulse has a transmission rate of 1, 5, and 10 Gbps. Both before and after the amplification, the output level has been monitored using a spectrum analyzer.

Designing a photo detector in a simulation environment involves understanding the key parameters that affect its performance, such as responsivity, dark current, bandwidth, quantum efficiency, and noise characteristics. Responsivity measures how efficiently the photo detector converts incident optical power into an electrical current:

$$R = \frac{I_{ph}}{P_{opt}} = \frac{\eta q}{h\nu} = \frac{\eta\lambda}{1.24} \tag{59}$$

where v is the optical frequency (in Hz), λ is the wavelength of the incident light (in micrometers), h is Planck's constant (6.626×10^{-34}Js), q is the electron charge (1.602×10^{-19} C), and I_{ph} is the photocurrent (in amperes). All of these values are expressed as unitless ratios. The responsivity R (in A/W), for instance, can be computed at a wavelength of 1550 nm as

$$R \approx \frac{\eta 1550}{1.24}A/W \ \&\ \eta = 0.8\times10^{-3} \tag{60}$$

$$R = \frac{(0.8\times10^{-3})(1550)}{1.24} \approx 1A/W \tag{61}$$

Sensitivity is a critical metric in simulation software photo detector design that measures the lowest optical power needed to reach a given performance level, usually expressed in terms of BER. Analyzing the photo detector's reaction to various input optical powers while taking noise and the necessary Signal-to-Noise Ratio (SNR) into consideration will reveal the sensitivity. The general formula for figuring out a photo detector's sensitivity P_{min} is

$$P_{\min} = \frac{Q\sigma_n}{R} \tag{62}$$

where σ_n is the normal deviations of the noise current (total noise, including thermal noise, shots, noise, etc.), R is the photo detector's responsivity, Q is the quality factor associated with the intended BER, and P_{min} is the lowest detectable optical power, or sensitivity. Quantum efficiency, which is determined by the percentage of incoming photons that produce electron-hole pairs, which subsequently contribute to the photocurrent.

$$\eta = \frac{No.of\ electron-hole\ pairs\ generated}{No.of\ incident\ photons} \tag{63}$$

The photocurrent generated by the photo detector is given by

$$I_{ph} = RP_{opt} = \frac{\eta q P_{opt}}{h\nu} \tag{64}$$

Usually brought on by the thermal production of carriers, dark current is a tiny current that passes through a photo detector even when there is no light.

$$I_d = I_s(e^{\frac{qV}{kT}} - 1) \tag{65}$$

Here, k is Boltzmann's constant (1.38×10^{-23} J/K), T is the absolute temperature (in Kelvin), I is the reverse of the saturation current (in amperes), and Vis is the applied backward bias voltage (in volts). There are several different types of noise that can occur in a photo detector, including thermal noise, shot noise, and dark current noise. The overall current of noise is given as

$$i_n = \sqrt{i_{sh}^2 i_{thermal}^2 + i_{dark}^2} \tag{66}$$

In this case, B is the photo detector's bandwidth (in Hz), R_L is the load resistance (in ohms), $i_{thermal}$ is the thermal noise current (−4 kTB/RL), and i_{dark} is the dark current noise (−2 q Id B). A photo detector's transit-time limit and RC time constant define its bandwidth.

$$B = \frac{1}{2\pi R_L C_j} + \frac{\nu_{sat}}{d} \tag{67}$$

Here, V_{sat} is the carrier saturation velocity (in m/s), d is the depletion area width (in meters), C_j is the junction capacitance (in farads), and R_L is the load resistance (in ohms). How well the photo detector can separate the signal from noise is indicated by the SNR.

$$SNR = \frac{I_{ph}}{i_n} \tag{68}$$

In optical communication systems, the Q-factor is mathematically related to the BER as:

$$BER = \frac{1}{2} erfc \frac{Q}{\sqrt{2}} \tag{69}$$

The simulation result of Q-factor is 32.1. Substitute the value in the formula,

$$BER = \frac{1}{2} erfc \frac{32.1}{\sqrt{2}} = 2.21e^{-226} \tag{70}$$

The comparison between the simulation and mathematical results shows a very close agreement, with the simulated BER value of $6.8e^{-227}$and the analytically calculated BER of $2.21e^{-226.}$ Although a slight variation exists, this difference is negligible and can be attributed to numerical precision limits and the exponential sensitivity of BER to the Q-factor at such high values. Importantly, both results confirm the best performance of the proposed system, demonstrating an exceptionally low error probability that is practically unachievable through direct measurement but highly reliable through extrapolation. This close correlation between analytical and simulation outcomes validates the robustness of the model and reinforces the accuracy of the system design.

Based on the above analytical expression, the simulation parameters for modulator with laser source, optical amplifier, fiber cable, photo detector and FBG has been chosen as listed in Tables 2 to 7 as follows.

Table 2. Simulation parameter setup of CW Laser

Parameter	Value
CW Frequency	193.1 THz
CW Line width	10 MHz
Optical Power	0,5,10 and 15 dBm

Table 3. Simulation parameter setup of DD-MZM

Parameter	Value
Extinction Ratios	20 dBm
RF Switching and bias Voltage	4 V
Bias Voltage in DD-MZM	0 V
Insertion Loss	5 dB
Bias Voltage1	0 V
Bias Voltage2	2 V

Table 4. Simulation parameter setup of FBG

Parameter	Value
Frequency	193.1THz
Effective Index	1.45
Length	2 mm
Apodization Function	Uniform
Modulation AC	0.0001

Table 5. Simulation parameter setup of Optical Fiber

Parameter	Value
Fiber Length	10 to 140 Km
Attenuation	0.2 dB/Km
Reference Wavelength	1550nm
Dispersion	16.75 ps/nm/km
Dispersion Slope	0.075 ps/nm^2/km
Differential Group Delay	0.2 ps/km
Effective Area	80 um^2

Table 6. Simulation parameter setup of Optical Amplifier

Parameter	Value
Amplifier Gain	20 dB
Noise Figure	4 dB

Table 7. Simulation parameter setup of Photo Detector

Parameter	Value
PD Responsivity	1 A/W
PD Dark Current	10 nA
Thermal Noise	1e^{-22} W/Hz

After being processed by a Bessel, an optical filter working at 193.1 THz with a bandwidth of 20 GHz, the single-mode fiber sending signal is sent to the photo detector, which is the main component and uses the "photoelectric effect" for converting the optical signal to an electrical signal that is converted into a mm-wave at GHz. The signal was further filtered using a Bessel optical filtering process, and then it was examined using the BER analyzer, 3R generator, RF and optical spectrum, that is, and eye diagram analysis software. The encoded message is transferred via an arcsine pre-distortion in order to compensate for the modulation nonlinearity and improve the transmitted signal amplitude. The RoF circuit configuration with the pre-distortion generator is shown in Fig 7(b). The dispassion compensation conceptual diagrams according to pre- and post-FBG are displayed in Figs. 7(c) and (d).

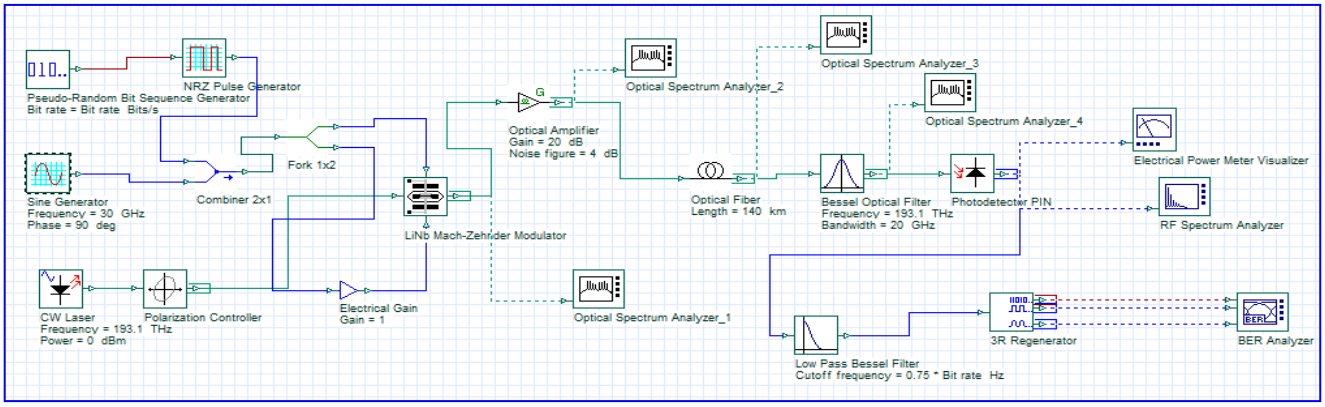

(a)

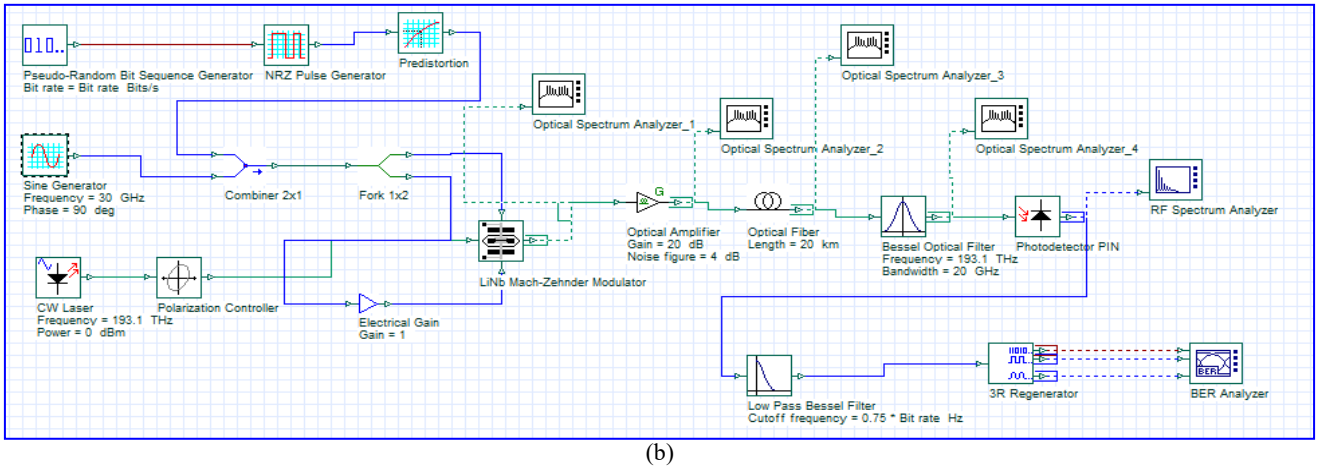

(b)

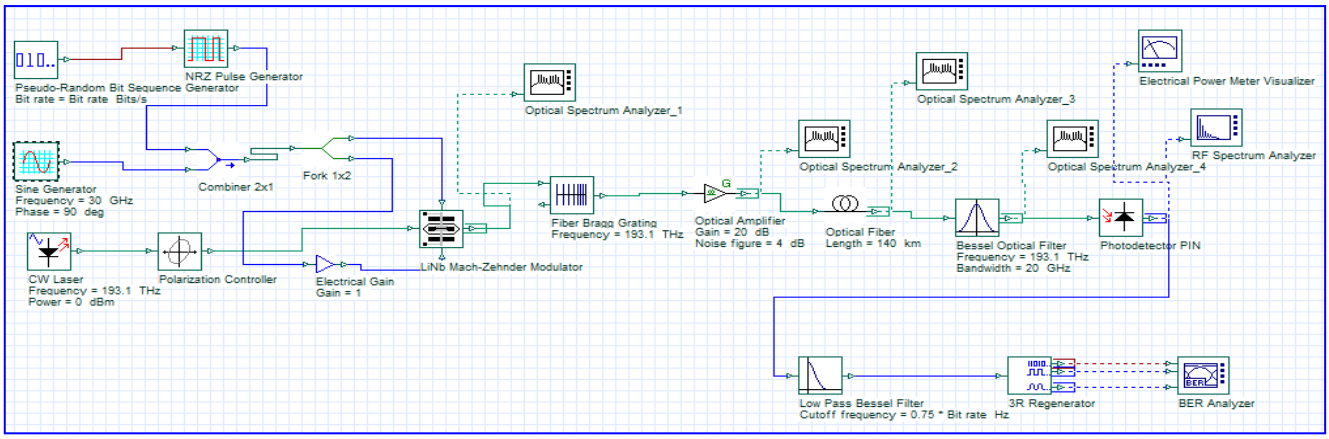
Pseudo-Random Bit Sequence Generator
Bit rate = Bit rate Bits/s
NRZ Pulse Generator
Sine Generator
Frequency = 30 GHz
Phase = 90 deg
Combiner 2x1
Fork 1x2
CW Laser
Frequency = 193.1 THz
Power = 0 dBm
Polarization Controller
Electrical Gain
Gain = 1
LiNb Mach-Zehnder Modulator
Optical Spectrum Analyzer_1
Fiber Bragg Grating
Frequency = 193.1 THz
Optical Amplifier
Gain = 20 dB
Noise figure = 4 dB
Optical Spectrum Analyzer_2
Optical Fiber
Length = 140 km
Optical Spectrum Analyzer_3
Bessel Optical Filter
Frequency = 193.1 THz
Bandwidth = 20 GHz
Optical Spectrum Analyzer_4
Electrical Power Meter Visualizer
RF Spectrum Analyzer
Photodetector PIN
Low Pass Bessel Filter
Cutoff frequency = 0.75 * Bit rate Hz
3R Regenerator
BER Analyzer

(c)

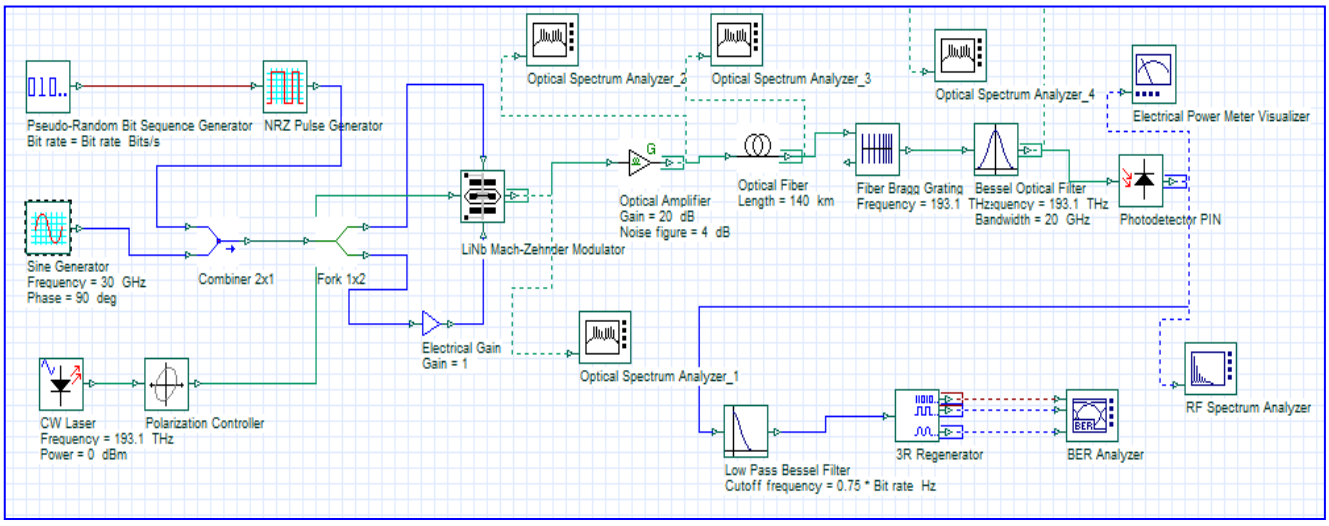
Pseudo-Random Bit Sequence Generator
Bit rate = Bit rate Bits/s
NRZ Pulse Generator
Sine Generator
Frequency = 30 GHz
Phase = 90 deg
Combiner 2x1
Fork 1x2
CW Laser
Frequency = 193.1 THz
Power = 0 dBm
Polarization Controller
Electrical Gain
Gain = 1
LiNb Mach-Zehnder Modulator
Optical Spectrum Analyzer_2
Optical Spectrum Analyzer_3
Optical Amplifier
Gain = 20 dB
Noise figure = 4 dB
Optical Fiber
Length = 140 km
Fiber Bragg Grating
Frequency = 193.1 THz
Optical Spectrum Analyzer_4
Bessel Optical Filter
Frequency = 193.1 THz
Bandwidth = 20 GHz
Electrical Power Meter Visualizer
Photodetector PIN
Optical Spectrum Analyzer_1
RF Spectrum Analyzer
Low Pass Bessel Filter
Cutoff frequency = 0.75 * Bit rate Hz
3R Regenerator
BER Analyzer

(d)

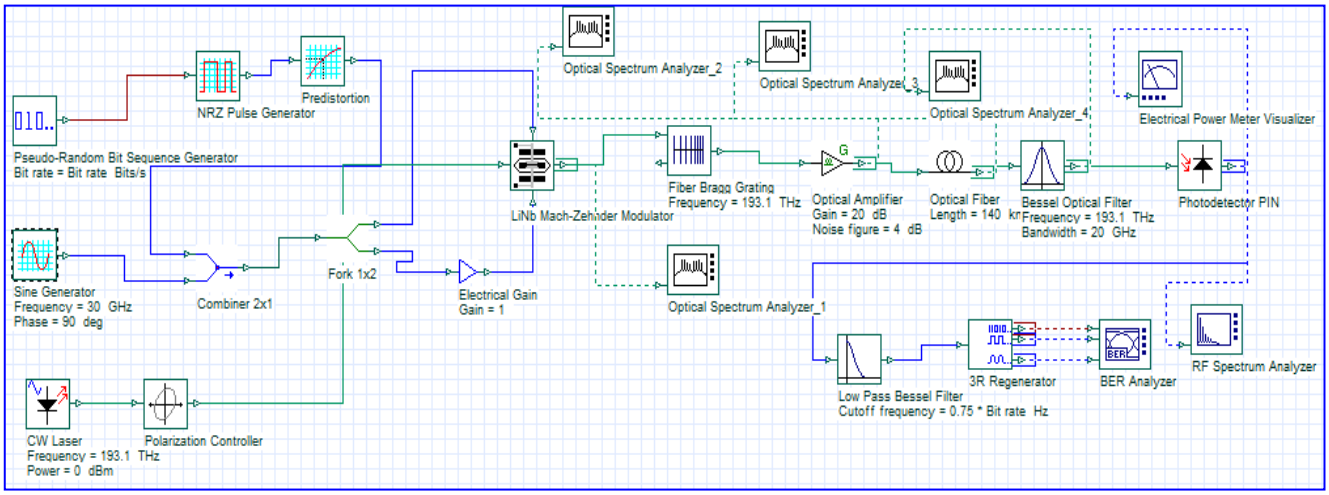
Pseudo-Random Bit Sequence Generator
Bit rate = Bit rate Bits/s
NRZ Pulse Generator
Predistortion
Sine Generator
Frequency = 30 GHz
Phase = 90 deg
Combiner 2x1
Fork 1x2
CW Laser
Frequency = 193.1 THz
Power = 0 dBm
Polarization Controller
Electrical Gain
Gain = 1
LiNb Mach-Zehnder Modulator
Optical Spectrum Analyzer_2
Optical Spectrum Analyzer_3
Fiber Bragg Grating
Frequency = 193.1 THz
Optical Amplifier
Gain = 20 dB
Noise figure = 4 dB
Optical Fiber
Length = 140 km
Optical Spectrum Analyzer_4
Bessel Optical Filter
Frequency = 193.1 THz
Bandwidth = 20 GHz
Electrical Power Meter Visualizer
Photodetector PIN
Optical Spectrum Analyzer_1
RF Spectrum Analyzer
Low Pass Bessel Filter
Cutoff frequency = 0.75 * Bit rate Hz
3R Regenerator
BER Analyzer

(e)

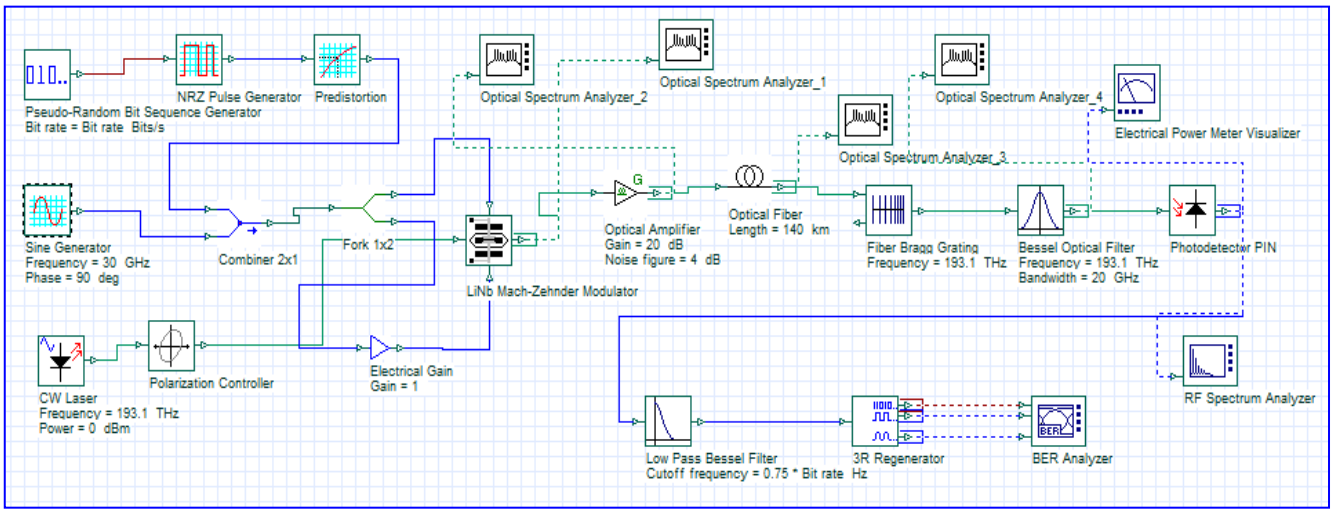

(f)

Fig. 7. Diagrammatic representation of a classical mm-wave RoF simulation model. (a) Basic (b) Pre-distortion (c) pre-FBG (d) Post-FBG (e) Pre-distortion and pre-FBG (f) Pre-distortion and post-FBG (colour online)

Figs. 7(e) and 7(f) depict the system layout for integrating the two pre-distortion devices and the two dispersion compensations Pre-FBG and Post-FBG, respectively. The input radio frequency signal is generated at 30 and 60 GHz by a sine generator, also referred to as a local oscillator, after the data stream has been compressed and the corresponding NRZ coding techniques have been improved. Regular pre- and post-FBG use has been made of the optical filter at 193.1 THz with a 5 GHz bandwidth.

5. Results and discussion

The system's performance was examined for transmission rates of 1, 5, and 10 Gbps using the fiber length of 140 Km. At large bit rates, modulation format, kind of dispersion correction mechanism, as well as channel power are considered as the crucial parameter to analyse.

The NRZ modulation results in a substantial eye closure penalty towards end channels. After analysing the spectrum of the optical fiber's output as a result of the DD-MZM modulator for all six modules, pre-FBG was selected for additional parametric study due to its high Q-factor, received power, lower BER, and higher threshold in the generated mm-wave. In a RoF link, Inter-Modulation Distortion (IMD) brought from Electro-Optic Modulators (EOMs) along with photo detectors might in fact impact the simulation findings, particularly when examining the system's overall performance. The quality of the signal and, consequently, the precision of the simulation results can be affected by the non-linearity's and harmonics introduced by these distortions. The dispersion effects and IM may interact, making simulation more difficult.

Fig. 8 (a) shows the simulation result of the optical spectrum analyzer after optical fiber transmission and Fig. 8 (b) and (c) is the same spectrum after photo detector that is converted from an optical signal to an electrical millimeter signal at 30 and 60 GHz. Fig. 8 (d) and (e) is a BER analyzer output for Q-factor and log of BER signal. Every parametric study is run with different fiber lengths and data speeds of 1, 5, and 10 Gbps. Fig. 9(a) through (c), depicts the recommended pre-FBG-mm-wave in the RoF using NRZ coding. High Q-factor with a nearly zero BER for three different 10 Gbps data rates at the input power level of 15 dBm has been noticed in Fig. 9 (a) and it outperforms the other five modules created in this proposal for its fiber length variation between 20 to 140 Km. The pre-FBG-mm-wave RoF method exhibits a maximum Q-factor value of 250 for a distance of 20 Km. At 140 Km, it outperforms all other schemes with a Q-factor of 25.3 and a BER of $5.7 \times e^{-120}$ because of its smooth decline in the rate of Q-factor versus optical fiber length. Compared to the module with the pre distorter block, the ones designed with the pre- and post-FBG displayed a higher Q-factor. When paired with pre distortion, the Q-factor of the RoF before and after FBG mm wave generation has been observed to deteriorate.

Fig. 9 (b) and (c) shows the superior performance of the module using the FBG mm wave unit and, contrasted with all the other modules, including pre-distortion at a date rate of 5 Gbps as well as 10 Gbps, respectively with slope of reduction in Q-factor from 80 to 45. When compared to each of the three-side bands produced, the carrier frequency offers the most OSSR at 9.2 dBm in an optical spectrum analyzer.

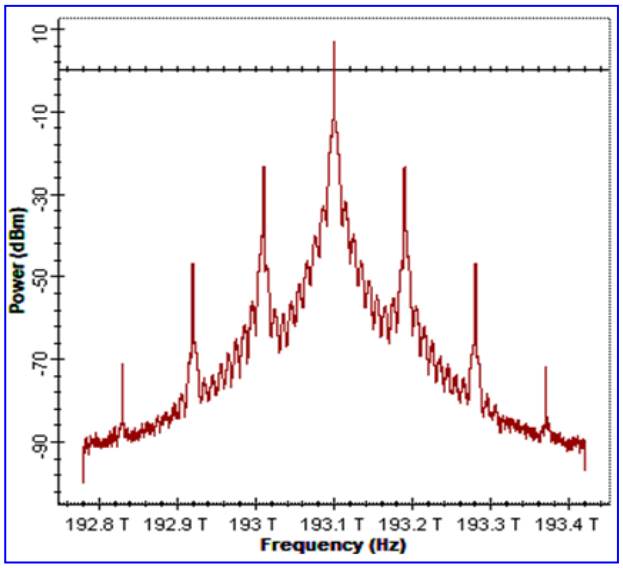

(a)

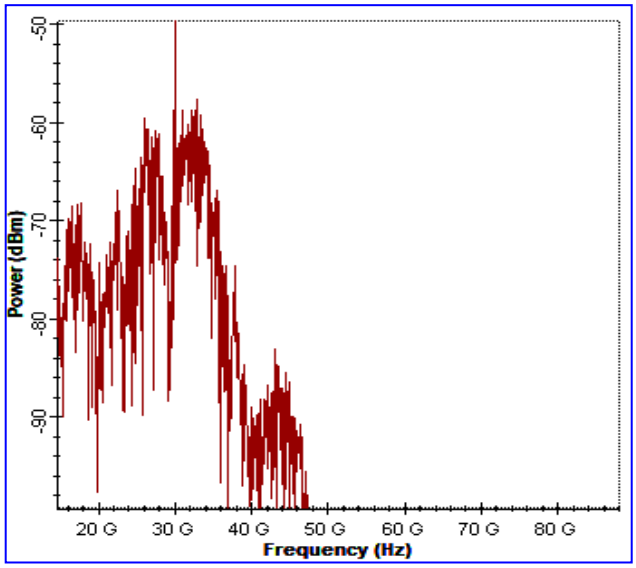

(b)

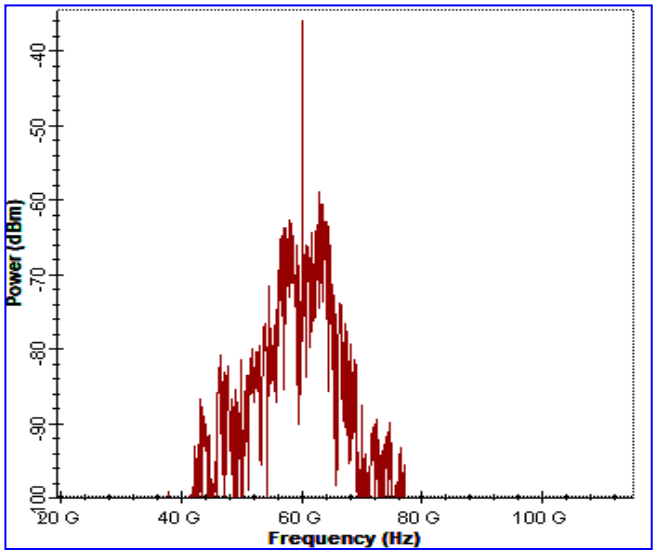

(c)

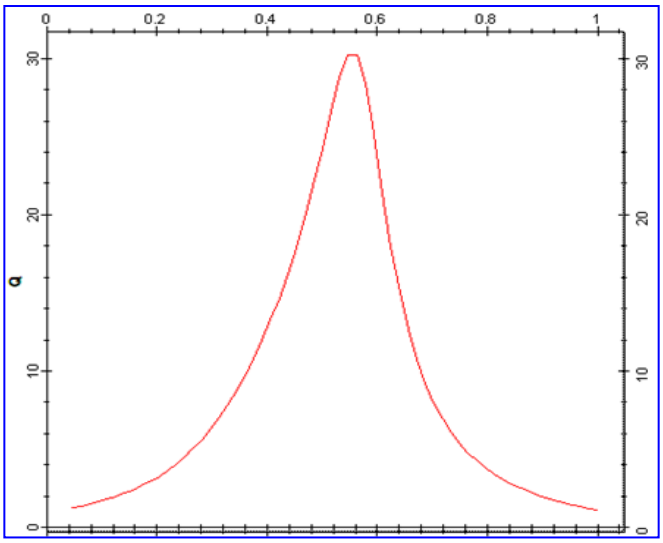

(d)

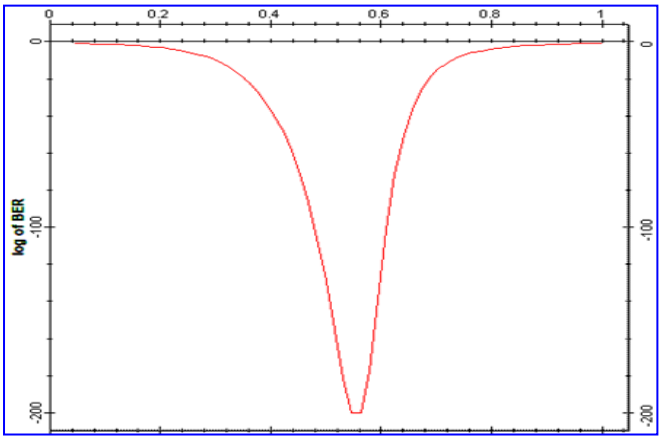

(e)

Fig. 8. Simulation results (a) optical spectrum at fiber end mm-wave RF spectrum at (b) 30 GHz (c) 60 GHz (d) Q-factor (e) BER (colour online)

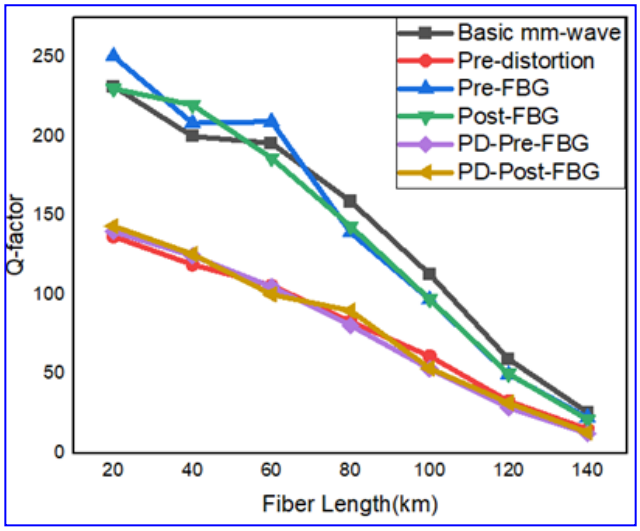

(a)

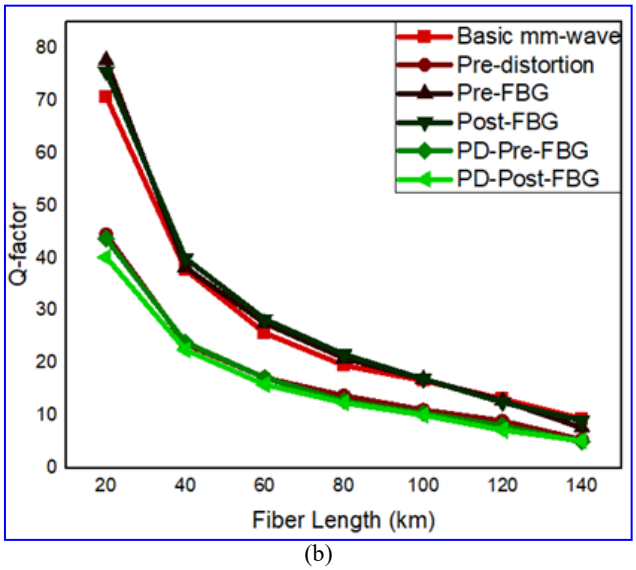

(b)

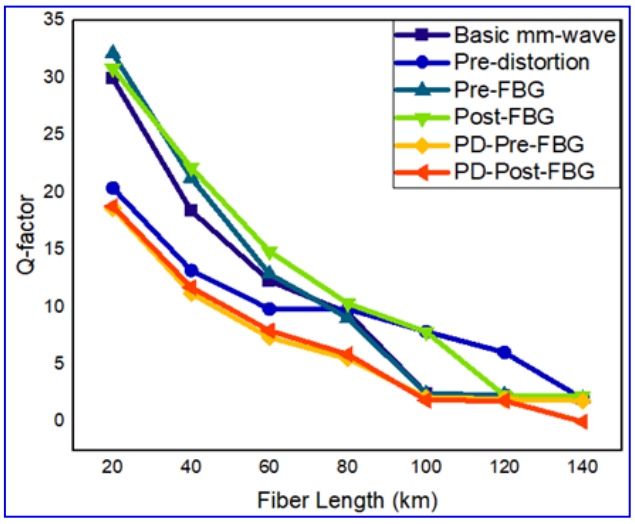

(c)

Fig. 9. Fiber length Vs Q factor using various data rates (a) 1 Gbps (b) 5 Gbps (c) 10 Gbps (colour online)

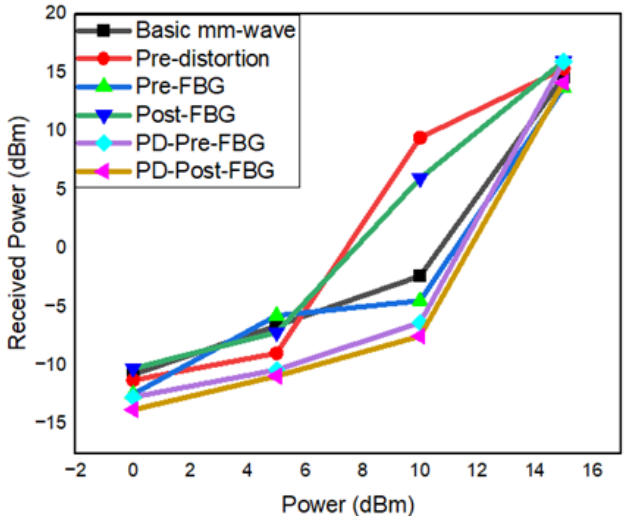

(a)

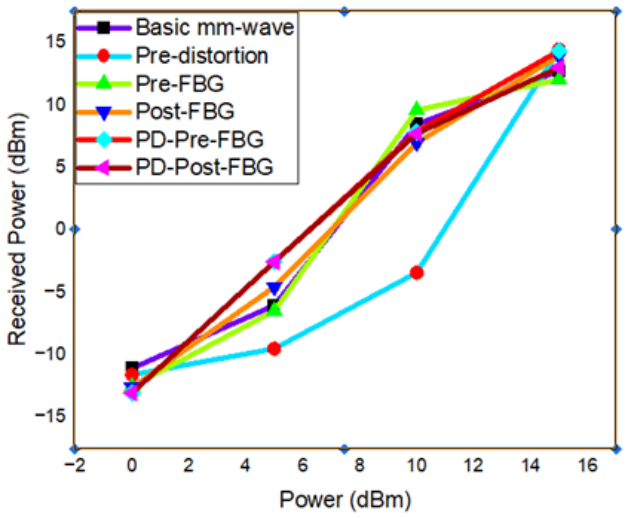

(b)

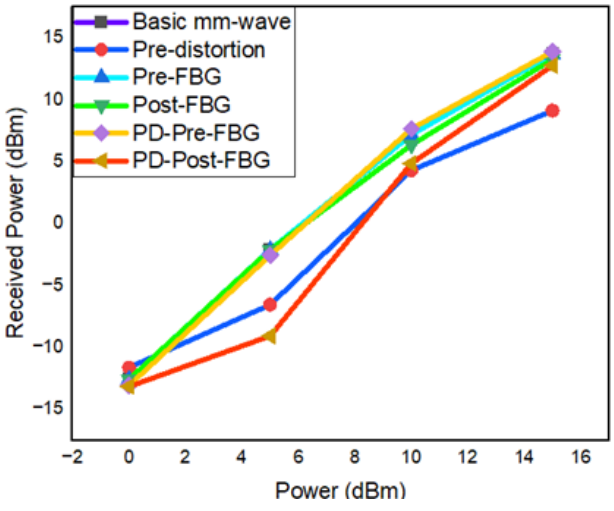

(c)

Fig. 10. Input laser power Vs RF spectrum output power with different data rates (a) 1 Gbps (b) 5 Gbps (c) 10 Gbps (colour online)

There is no much of a variation in eye height depending on data rate. Lastly, a plot of the relationship between the power at the end of the RF spectrum analyser and the input supplied at the CW laser has been compared, as illustrated in Fig. 10. It shows that while there is little difference in the output power, the linear operation of the RoF system using a laser source has improved with an increased data rate. There is a significant variation in nonlinearity observed in a result at pre-distortion as well as linearity promised in a RoF with pre-FBG. Fig. 10 (a) to (c) over the information rate at 1, 5, and 10 Gbps, correspondingly and shows that close linearity is being attained in all modules other than RoF system in pre distortion. These data together demonstrated that the suggested methods for mm-wave in RoF system using fiber optical transmission produce the RF spectrum around -11 dBm power levels. When compared to each of the three-side bands created, the carrier frequency in this model still has the maximum RFSSR at -66 dBm in the RF spectrum analyzer.

The technical researched parameters have been compared in Table 8 in order to validate the pre-FBG for its greater efficiency regarding the quality element, eye height, and the power that was obtained parameter values compared to the other five modules. Pre-FBG outperforms all other model topologies in the present investigation with a Q-factor of about 32.135 and BER of $6.8e^{-227}$ at a receiving power of -11.0241 dBm, according to the computations for the six models.

As shown in Table 9, the performance comparison of different modulation schemes for RoF and RoFSO links shows that the three-band serial and parallel modulator configuration achieves an aggregate capacity of 30 Gbps (10 Gbps per band) over 50 Km, while reverse modulation supports 2.5 Gbps up to 116 Km and 10 Gbps up to 78 Km. Similarly, hybrid modulation extends the reach to 119 Km at 2.5 Gbps and 76 Km at 10 Gbps. In contrast, the proposed system, however, outperforms all existing approaches by delivering 10 Gbps over 140 Km, thereby demonstrating enhanced transmission distance without compromising data rate.

Table 8. Simulation results of proposed six modules of RoF system

Techniques	Q-Factor	BER	Threshold	Received Power (dBm)
Basic	29.955	1.86×10^{-197}	0.00520	-12.560
Pre-distortion	20.3988	8.4×10^{-93}	0.00417	-11.605
Pre-FBG	**32.135**	$\mathbf{6.8\times10^{-227}}$	**0.00496**	**-11.024**
Post-FBG	30.8279	5.5×10^{-209}	0.00453	-12.040
PD-pre-FBG	18.6281	9.34×10^{-78}	0.00428	-13.055
PD-post-FBG	18.7936	4.261×0^{-79}	0.00437	-13.141

Table 9. Comparison between the proposed systems

Modulations	Data Rate (Gbps)	Transmission distance (Km)
Three-Band Serial and Parallel Modulators [25]	30 (10 Gbps per band)	50
Reverse Modulation [27]	2.5	116
	10	78
Hybrid Modulation [27]	2.5	119
	10	76
DD-MZM (This Work)	**10**	**140**

Table 10 presents a comparative analysis of the proposed work against previously reported studies. Table 2 presents a comparative analysis of the proposed work against previously reported studies. Over the past few years, several researchers have explored the performance of RoF systems at different data rates and transmission distances. Singh et al. (2016) achieved 5 Gbps over 60 Km with a Q-factor of 15 and BER of 1×10^{-10}, while Yang et al. (2017) extended the distance to 100 km at 2.5 Gbps but obtained a lower Q-factor of 12 with BER of 1×10^{-9}. Bi et al. (2018) increased the capacity to 10 Gbps over 80 Km, recording a Q-factor of 13.5. Meena M. L. et al. (2019) enhanced system efficiency by reporting 10 Gbps over 60 Km with a much-improved Q-factor of 24.4 and BER of 9.1×10^{-13}. More recent works, such as Muhammad Towfiqur et al. (2023), achieved 2.5 Gbps over 20 Km with BER of 1×10^{-9}, whereas Alyaa Ali Hameed (2024) reached 5 Gbps over 135 Km but only achieved a Q-factor of 7.1 with BER of 5.02×10^{-14}. In comparison, this work demonstrates significant improvement, enabling 10 Gbps transmission over 140 Km of SMF with an exceptional maximum Q-factor of 32.1 and an ultra-low BER of 6.8×10^{-227}, confirming the transmission reach and signal integrity of the proposed pre-FBG-based RoF system for long-haul, high-capacity communication.

Table 10. Comparison between our suggested system and current mm- wave system

Author	Data Rate (Gbps)	SMF (Km)	Q-factor	BER
Singh et al. (2016)	5	60	15	$1e^{-10}$
Yang et al. (2017)	2.5	100	12	$1e^{-9}$
Bi et al. (2018)	10	80	13.5	$1e^{-9}$
Meena ML et al. (2019)	10	60	24.4	$9.1e^{-13}$
Muhammad Towfiqur et al. (2023)	2.5	20	-	10^{-9}
Alyaa Ali Hameed (2024)	5	135	7.1	$5.02e^{-14}$
This Work	**10**	**140**	**32.1**	**$6.8e^{-227}$**

6. Conclusion

This work has demonstrated the effectiveness of the pre-FBG-based mm-wave generation technique in a RoF system using NRZ coding. Simulation results confirm that with carrier frequencies of 30 GHz and 60 GHz at 10 Gbps, the system achieves excellent performance with a maximum Q-factor of 32.1 over 140 Km of fiber. The graphical parameters for Q-factor (32.1), and BER ($6.8e^{-227}$), have been successfully verified, confirming the reliability and effectiveness of the proposed pre-FBG-based mm-wave RoF system. The proposed design provides a simple, low-cost, and reliable solution for long-distance (140 Km), high-frequency (60 GHz) transmission. The results highlight that the pre-FBG-mm-wave RoF scheme not only ensures strong signal quality and stability but also offers a scalable architecture suitable for future high-capacity and long-distance wireless communication networks. The demonstrated architecture can be extended to support advanced modulation formats, paving the way for 20 Gbps and beyond optical wireless transmission in next-generation broadband networks.

Statements and declarations

Funding: The authors declare that no funds, grants, or other support were received during the preparation of this manuscript.

Competing Interests: The authors have no relevant financial or non-financial interests to disclose.

Financial interests: The authors declare they have no financial interests

Author Contributions: All authors contributed to the study conception and design. Material preparation, data collection was performed by [Krishna Mari Selvi T.] and analysis were performed by [Krishna Mari Selvi T.] and [Suganthi Santhanam]. The first draft of the manuscript was written by [Krishna Mari Selvi T.] and editing and final version prepared by [Suganthi Santhanam]. All authors commented on previous versions of the manuscript, read and approved the final manuscript.

Data Availability: The datasets generated during and/or analyzed during the current study are available from the corresponding author on reasonable request.

References

[1] Robi Darwis, Octarina Nur Samijayani, Ary Syahriar, Indrawan Arifianto, Universal Journal of Electrical and Electronic Engineering **6**(3), 159 (2019).
[2] Fabrice Mfuamba Kabonzo, Yunfeng Peng, Journal of Computer and Communications **4**(3), 1 (2016).
[3] Sevan H. Ali, Raghad Zuhair Yousif-Al-Maqddic, Soft Computing **28**, S787 (2024).
[4] Muhammad Usman Hadi, Jacopo Nanni, Jean-Luc Polleux, Pier Andrea Traverso, Giovanni Tartarini, Optical and Quantum Electronics **51**, 205 (2019).
[5] K. Manjushree, U. M. Roy, 2019 Workshop on Recent Advances in Photonics (WRAP), Guwahati, India, pp. 1-3 (2019).
[6] Asha Balhara, Sandeep Dahiya, Journal of Optics **52**, 1461 (2023).
[7] Chaluvadi V. Naga Bhaskar, Subhradeep Pal, Prasant Kumar Pattnaik, J. Opt.-UK **25**, 125701 (2023).
[8] Dedi Irawan, Azhar, Khaikal Ramadhan, Journal of Research in Science Education **8**, 992 (2022).
[9] Shaymaa R. Tahhan, Abdulla K. Abass, Mudhafar H. Ali, Journal of Communications **13**(3), 108 (2018).
[10] Nazmi A. Mohammed, Mohammad Solaiman, Moustafa H. Aly, Applied Optics **53**(29), H239 (2014).
[11] N. Basil, M. Moutaz, Informatics on Applied Machines Electrical Electronics Computer Science and Communication Systems **2**(1), 01 (2021).
[12] M. L. Meena, Raj Kumar Gupta, Optik **188**, 212 (2019).
[13] Yosef T. Aladadi, Firman Abas, Mohammed Alresheedi, Journal of the European Optical Society – Rapid Publications **1**(12), 1 (2016).
[14] G. Karpagarajesh, Alice Blessie, R. Santhana Krishnan, Journal of Microelectronics, Electronic Components and Materials **51**(4), 215 (2021).
[15] Tamer F. Hussein, M. R. M. Rizk, Moustafa H. Aly, Journal of Optical and Quantum Electronics **51**, 1 (2019).
[16] J. Ranathive, K. Vinoth Kumar, Ahmed Nabih Zaki Rashed, Mohammed Salah F. Tabbour, Journal of Optical Communications **43**(4), 611 (2022).
[17] Deepika Meena, M. L. Meena, Optical and Wireless Technologies 29-36 (2020).

doi: 10. 1007 / 978-981-13-6159-3_4
[18] Muhammad Towfiqur Rahman, Shah Murtaza Rashid Al Masud, Tasnim Sabiha, Mushfiqur Rahman, International Journal of Microwave & Optical Technology **18**(4), 444 (2023).
[19] Khurram Karim Qureshi, Abdul Rehman Qureshi, Musab G. Magam, Laiq Jamal, Journal of Optical Communication **44**, (2020). doi: 10.1515/joc-2020-0074.
[20] Alyaa Ali Hameed, Journal of Al-Azhar University Engineering Sector **19**(71), 748 (2024).
[21] Christina Lim, Chathurika Ranaweera, Yijie Tao, Ampalavanapillai Nirmalathas, Sampath Ediringhe, Lena Wosinska, Journal of Lightwave Technology **43**, 1525 (2025).
[22] Toshiaki Kuri, Handbook of Radio and Optical Networks Convergence, Springer (2024). doi:10.1007/978-981-97-2282-2_40.
[23] Ruben Altuna, Yongmin Jung, Periklis Petropoulos, Carmen Vazquez, Laser and Photonics Reviews **18**, 2400157 (2024).
[24] M. A. Arroyave, B. Behera, F. Cavanna, A. Feld, F. Guo, A. Heindel, C. K. Jung, K. Koch, D. Leon Silverio, D. A. Martinez Caicedo, Journal of Instrumentation **19**, P10019 (2024).
[25] Richa Bhatia, Saurabh Prakash, Ekta Saini, J. Optoelectron. Adv. M. **21**(1-2), 64 (2019).
[26] Prabu Krishnan, Utsav Jana, Balaji K. Ashokkumar, IET Communications **12**(16), 2046 (2018).
[27] Richa Bhatia, Saurabh Prakash, Ekta Saini, International Journal of Communication Systems **32**, e3848 (2018).
[28] Luis Vallejo, Omaro Fawzi Abdelhamid Gonem, Wei Jin, Roger Philip Giddings, Lin Chen, Yi Huang, Journal of Lightwave Technology **43**(6), 2624 (2025).
[29] Lauryn P. Smith, Charles A. Lynch, C. Alex Kaylor, L. Alberto Campos, Lin Cheng, Stephen E. Ralph, IEEE Access **13**, 132067 (2025).
[30] Vicente Fito, Raúl Ortiz, Maria Morant, Laura Mercadé, Alejandro Martínez, Roberto Llorente, IEEE Photonics Journal **17**(1), Art. No. 7200409 (2025).
[31] Yitong Li, Jianguo Yu, Naibo Zhang, Kun Deng, Guangyao Yang, Ruiliang Song, IEEE Photonics Journal **17**(1), Art. No. 7300106 (2025).
[32] Yizhang Li, David P. Schaber, Hans H. Brunner, Jan Hesselbarth, Christian Bluemm, IEEE Microwave and Wireless Technology Letters **35**(7), 1013 (2025).
[33] Guangxu Shen, Bijing Wen, Zizhe He, Na Ji, Wenjie Feng, Wenquan Che, IEEE Microwave and Wireless Technology Letters **35**(6), 686 (2025).

*Corresponding authors: suganthis.ece@krct.ac.in, krishna1996mari@gmail.com